ADVANCED MATERIALS
www.advmat.de

Physically Flexible, Rapid-Response Gas Sensor Based on Colloidal Quantum Dot Solids

Huan Liu, Min Li, Oleksandr Voznyy, Long Hu, Qiuyun Fu, Dongxiang Zhou, Zhe Xia, Edward H. Sargent, and Jiang Tang**

Detection of toxic or hazardous gases has become increasingly important for environmental monitoring, personal safety protection, and industrial manufacturing. NO_2, one of the major hazardous gases released in vehicle exhausts and by fossil fuel combustion, not only causes severe respiratory problems in humans, including pulmonary edema, but also results in acid rain, threatening animals, plants, and the environment. Ideally a NO_2 sensor would be highly sensitive, rapid to respond and highly reversible, readily capable of being integrated with a variety of substrates, and would work at room temperature for low cost and ease of operation. Advanced gas sensor requirements also include being flexible and stretchable to enable smart electronics applications such as wearable gas detectors.[1]

Unfortunately, traditional chemiresistive sensors using semiconducting oxides, although they do show excellent sensitivity, rely on rigid substrates such as ceramics or quartz, and require operation in the 200–600 °C temperature range.[2] This high operating temperature raises both power consumption and safety issues. These limitations have motivated a large and fast-moving worldwide effort to produce rapid, sensitive, room-temperature-operating flexible gas sensors.[3]

Thanks to their large surface area and low-temperature processing, nanomaterials (including carbon nanotubes,[4] graphene,[5] and nanocrystalline SnO_2[6]) have been used to build flexible gas sensors by means of spin-coating,[7] ink-jet printing,[4a,5a] and transfer-printing[4b] onto various flexible substrates, including poly(ethylene terephthalate) (PET),[5a] polyimide (PI), and even paper.[4a] Ink-jet-printed carbon nanotubes on cellulosic substrates showed excellent selectivity and robustness with respect to aggressive vapor (Cl_2 and NO_2) detection, while their 5-minute response time is too sluggish for practical real-time sensing applications.[4a] Reduced graphene oxide printed onto a PET substrate showed a sensitive response in NO_2 detection, however, 254 nm UV light irradiation was required to recover the sensor owing to the strong chemisorption of NO_2 vapor upon the graphene surface.[5a] Electro-spun porous SnO_2 nanofibers enabled detection of NO_2 down to the parts per billion (ppb) level, however, their high operating temperature (350 °C) excludes their integration with most flexible substrates.[8]

In general, strong adhesion of gas molecules to the sensing material favors sensitive gas detection; however, strongly adsorbed molecules are difficult to remove and account for the slow recovery time of many gas sensors. We hypothesized that colloidal quantum dots (CQDs) — a highly tunable material — might offer the programmable materials properties needed to define a high-performance gas sensor that met simultaneously this demanding set of specifications. CQDs have a widely tunable bandgap and solution processability, and their application has been extensively explored in solar cells,[9] light detectors,[10] and light emitters.[11] Because CQDs are nanocrystals of a few nanometers in diameter, they have an extremely large surface-to-volume ratio capable of active interaction with target gas molecules.[12] They can be solution-processed at room temperature onto a wide variety of substrates,[13] enabling the usage of flexible and lightweight substrates. Attractively, there exist many degrees of freedom in CQD materials processing, including impurity doping[2b] and ligand exchange.[9a,14] These lead to versatile physical and chemical properties, with widely varying thickness and porosity of the CQD solid. Moreover, strong wave function leakage outside the CQD core suggests that their macroscopically measured electronic properties could sensitively report changes at their surface,[15] facilitating an excellent response upon the presence of specific gases.

In the work reported here, we have demonstrated for the first time a gas sensor based on PbS CQDs. We constructed the devices on paper substrates, resulting in flexible, rapid-response NO_2 gas sensors fabricated from the solution phase. The devices operate at room temperature and are highly sensitive and fully recoverable. We studied the mechanisms that enable these remarkable devices and found that the excellent access of gas molecules to CQD surfaces, realized by surface ligand removal, and the desirable binding energy of NO_2 with PbS CQDs were the key parameters that accounts for these devices' rapid and sensitive NO_2 detection.

PbS CQDs were synthesized and isolated according to the literature.[16] Powder X-ray diffraction (XRD) analysis confirmed that the products were cubic-lattice PbS (JCPDS 02–0699), and the sharp absorption excitonic peak indicated a narrow size distribution (Figure S1 in the Supporting Information). The average diameter was estimated to be 4.0 nm based on the Moreels method,[17] with a relative size dispersion of 7.5%.

Prof. H. Liu, M. Li, Prof. Q. Y. Fu, Prof. D. X. Zhou
School of Optical and Electronic Information
Huazhong University of Science and Technology
1037 Luoyu Road, Wuhan, Hubei, 430074, P. R. China
E-mail: fuqy@mail.hust.edu.cn
Dr. O. Voznyy, Prof. E. H. Sargent
Department of Electrical and Computer Engineering
University of Toronto
10 King's College Road, Toronto, Ontario M5S 3G4, Canada
L. Hu, Z. Xia, Prof. J. Tang
Wuhan National Laboratory for Optoelectronics
Huazhong University of Science and Technology
1037 Luoyu Road, Wuhan, Hubei, 430074, P. R. China
E-mail: jtang@mail.hust.edu.cn

DOI: 10.1002/adma.201304366

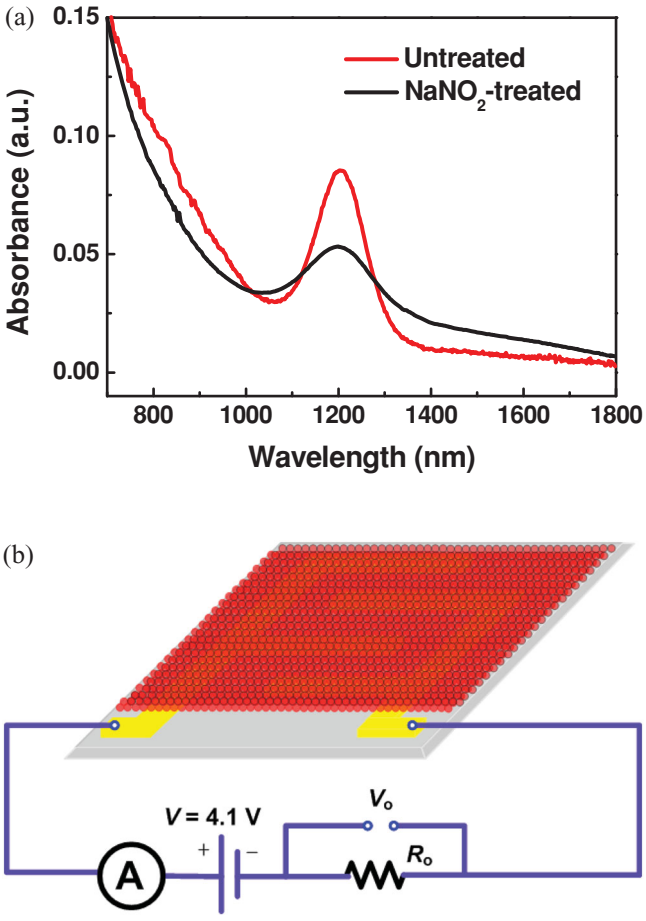

Figure 1. a) Absorption spectra of the untreated PbS CQD film and $NaNO_2$-treated PbS CQD film. b) Schematic device and measurement configurations. The top layer and bottom bars represent the PbS CQD film and Au electrodes, respectively.

The CQD films were spin-cast from 50 mg mL^{-1} PbS CQD octane solution. For the sensor fabrication, a 10 mg mL^{-1} sodium nitrite ($NaNO_2$) in methanol treatment was applied to produce a solid-state ligand exchange. Fourier transform infrared (FTIR) spectroscopy analysis (Figure S2a) of PbS CQD film fabricated on indium tin oxide (ITO) substrate revealed that the aliphatic C–H stretching bands at 2857–2920 cm^{-1} characteristic of the oleate ligand were significantly attenuated after the $NaNO_2$ treatment compared to the untreated films, suggestive of the removal of most oleate ligands, similar to other inorganic ion treatments.[9a,18] The excitonic peak remained after the $NaNO_2$ treatment, confirming conservation of strong quantum confinement in our PbS CQDs after $NaNO_2$ treatment(**Figure 1**a).[16] The surface elements and chemical states of PbS CQDs film after $NaNO_2$ treatment were examined using X-ray photoelectron spectroscopy (XPS) and data are included in the Supporting Information (Figure S2b). As expected, carbon, nitrogen and oxygen were detected on the sample, respectively due to oleate residual and CO_2 contamination, NO_2^- ligand binding to CQD surface, and NO_2^- ligand and surface oxidation. The atomic percentages for C, O, and N were 32.6%, 19.3%, and 2.6%, respectively, when Pb, S, C, O, and N were included in the calculation. Sulfur oxidation was observed because of air ambient processing, and the trace amount of Na originated from the $NaNO_2$ used for treatment.

For device fabrication, interdigital gold electrodes were first patterned onto substrates using radio frequency (RF) magnetron sputtering, followed by layer-by-layer spin-coating of PbS CQDs plus $NaNO_2$ treatment carried out at room temperature in air ambient. Figure 1b shows schematically the device and measurement configurations. For the sensor response measurement, a DC voltage of 4.1 V was applied and the voltage across (V_o) the signal resistor (R_o) was continuously recorded as the sensor sample was subjected to repeated target gas exposure and removal at room temperature (25 °C). The gas-sensing response S is defined as the ratio of the electrical resistance of the sensor in clean air (R_a) to that in the target gas (R_g, $S = R_a/R_g$). The response time ($T90$) is defined as the time required to reach 90% of the final response upon target gas exposure, and the recovery time ($T10$) as the time interval over which the sensor response drops to 10% of the stabilized response in the target gas when placed in clean air.

We compared device performance utilizing a variety of substrates, including Al_2O_3, PET, and paper. We show the response of each device to 50 ppm of NO_2 gas at room temperature in **Figure 2**a. For all devices, the sensor resistance significantly decreased after NO_2 exposure; when NO_2 gas was removed, the resistance increased and fully recovered its initial value. As depicted in Figure 2b, the response (recovery) time of sensors fabricated on Al_2O_3, PET, and paper were 11 s (45 s), 4 s (52 s) and 12 s (37 s), respectively, making these devices among the most rapid NO_2 gas sensors reported.[2b,19] All devices showed excellent reversibility and little appreciable baseline drift following multiple cycles. Neither illumination nor thermal treatment[20] was required to recover the sensor to baseline. The paper-based gas sensors showed the highest gas-sensing response S of 21.7 to 50 ppm of NO_2, while the responses for devices on ceramic and PET substrates were 13.0 and 3.5, respectively. The porous and rough nature of paper leads to higher film porosity (Figure S3, Supporting Information) and more efficient exposure of the CQD surfaces to the target gas molecules.

We provide more details of the dynamic response of the sensors upon repeated NO_2 exposure/removal cycles in Figure 2c. Six cycles were successively recorded, corresponding to NO_2 concentrations of 0.5, 2, 5, 10, 30, and 50 ppm, respectively. For all testing cycles, the resistance returned completely to its original value once NO_2 was pumped out. As shown in the inset in Figure 2c, sensor response depended approximately linearly on NO_2 gas concentration in the range 0.5–50 ppm, greatly simplifying the use in practical terms. On the other hand, we observed a response saturation when the NO_2 concentration exceeded 100 ppm. Through the least-squares method of fitting, we obtained the response slope in the linear regime to be 0.41 ppm^{-1} with a fitting quality $R^2 = 0.999$. The theoretical detection limit (for signal-to-noise ratio of 3) for NO_2 is approximately 84 ppb (for calculation details, see the Supporting Information).

Selectivity is another key parameter for gas sensors. Figure 2d shows the bar diagram of device response to different target gases (50 ppm) at room temperature. The sensors

Adv. Mater. **2014**,
DOI: 10.1002/adma.201304366

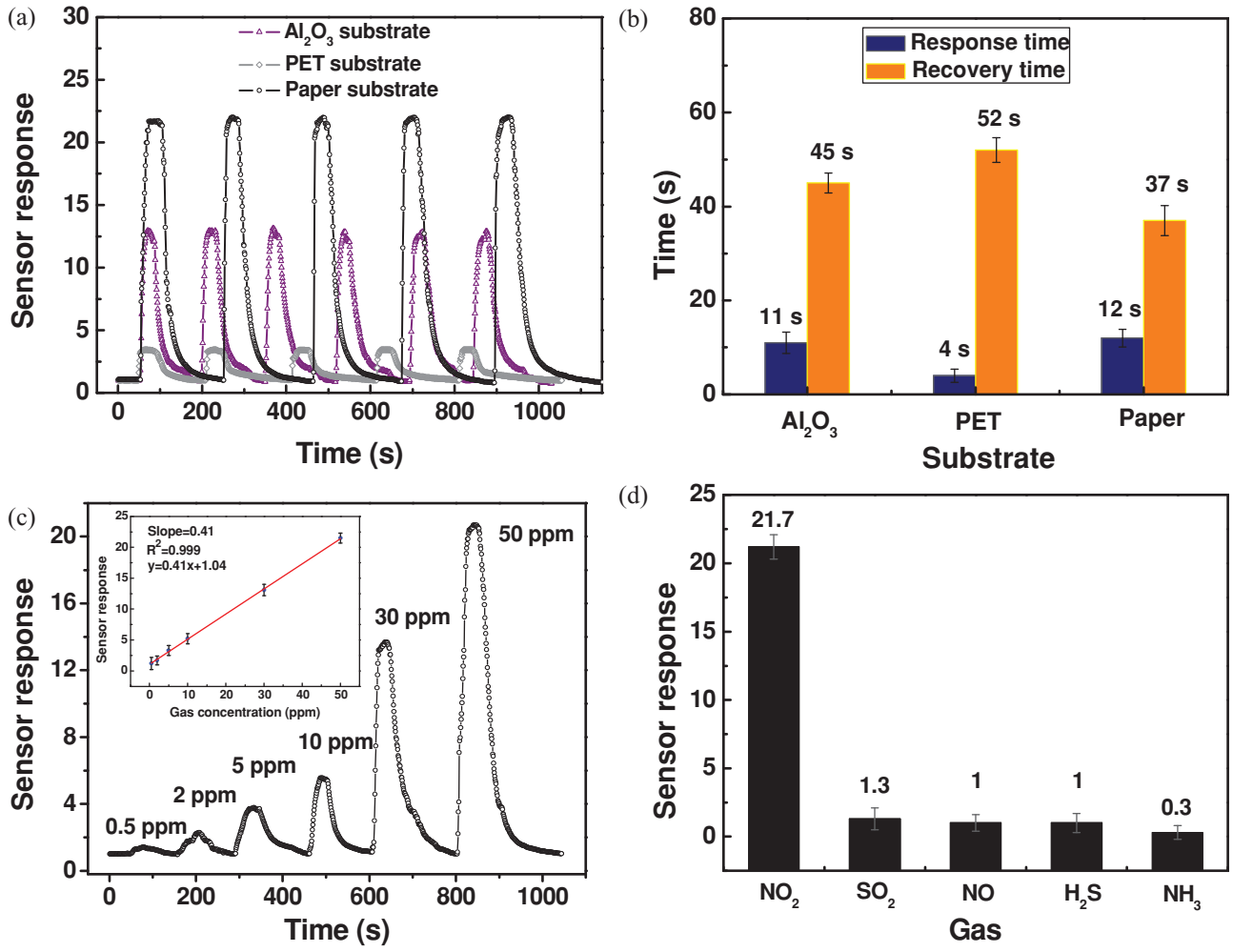

Figure 2. Response curves (a) and the response and recovery times (b) of PbS CQD gas sensors on different substrates (Al_2O_3, PET, and paper) to 50 ppm of NO_2 at room temperature. c) Response curves of the sensor to NO_2 of different concentrations. Inset: The sensor response depends linearly on NO_2 concentration. d) Response of PbS CQD sensor to different target gases (50 ppm) at room temperature. The values of response and response/recovery time in (b) and (d) and the inset in (c) were estimated using the data taken from 50 cycles of response curves (10 samples were fabricated using the same recipe and each sample was subject to 5 test cycles under same test conditions). The source of the error bars is the deviation of fabrication and test conditions.

exhibited high response to NO_2 gas and negligible response to SO_2, NO, H_2S, and NH_3. Reduced cross-sensitivity will minimize possible signal disturbance from intervening gas during practical application.

We now summarize the performance of our PbS CQD gas sensor and compare it with other NO_2 gas sensors reported in the literature (**Table 1**). All device performance figures are for NO_2 gas sensing at room temperature. The CQD sensors we reported here provide one order of magnitude faster response and recovery, and require no external impetus for recovery, in contrast to prior reports. These chemiresistive devices were made by spin-coating onto paper substrates, a simple and cost-effective approach compared to microfabrication[19] or thermal evaporation.[21] The paper substrates are inexpensive, lightweight and flexible, making them compatible with portable and wearable gas-monitoring systems.[21,22]

The rapid response of the CQD gas sensors may be attributed to excellent accessibility of CQD surfaces to gas molecules. The CQD film was only 80 nm thick, much thinner than most semiconductor oxide–based gas sensors, which are normally micrometers thick.[6b,25] The film was very porous, partly owing to significant volume shrinkage after ligand removal, and partly inherited from the coarse paper surface. These two features enable rapid diffusion of gas molecules into the bulk film, resulting in a fast initiation of the surface reaction on the PbS CQDs.

We further explored the bending and fatigue properties of our paper-based PbS CQD flexible gas sensor; the results were shown in **Figure 3**. The resistance of the sensor showed negligible changes at different bending angles up to 180° (Figure 3a). The inset shows the PbS CQD gas sensor being bent. Figure 3b shows the sensor response to 50 ppm of NO_2 when bent at different angles. The response and excellent reversibility of the sensor were fully retained at these bending angles. The robustness of the paper-based gas sensor with respect to repeated mechanical bending is further demonstrated in Figure 3c.

Table 1. Room-temperature NO_2 sensing performance of different sensor devices.

Materials	Method	Substrate	Gas concentration [ppm]	Sensor response[a)]	Response/Recovery time [s]	Detection limit [ppb]	Reference
PbS CQDs	Spin-coating	Paper	50	21.7	12/37	84	This work
Si nanowires	Transfer printing	Plastic	20	~30*	~75/–	–	23
Graphene	Micromechanical cleavage	Si wafers	1	~1.04*	~300/~220 (150 °C heating)	–	19
Graphene	Scooping-up	Mica	50	24.7	~500/~2500	3600	24
Organic heterojunction	Thermal evaporation	Si/SiO_2	30	7.7*	~1800/~3600	–	21
Carbon nanotubes	Inkjet printing	PET	50	~2.5*	~180/~600	~0.064	[4a]

[a)]Response values marked by an asterisk were recalculated for comparison according to the definition as the ratio of the higher to the lower value of the sensor resisitance in clean air (R_a) and in the target gas (R_g), respectively.

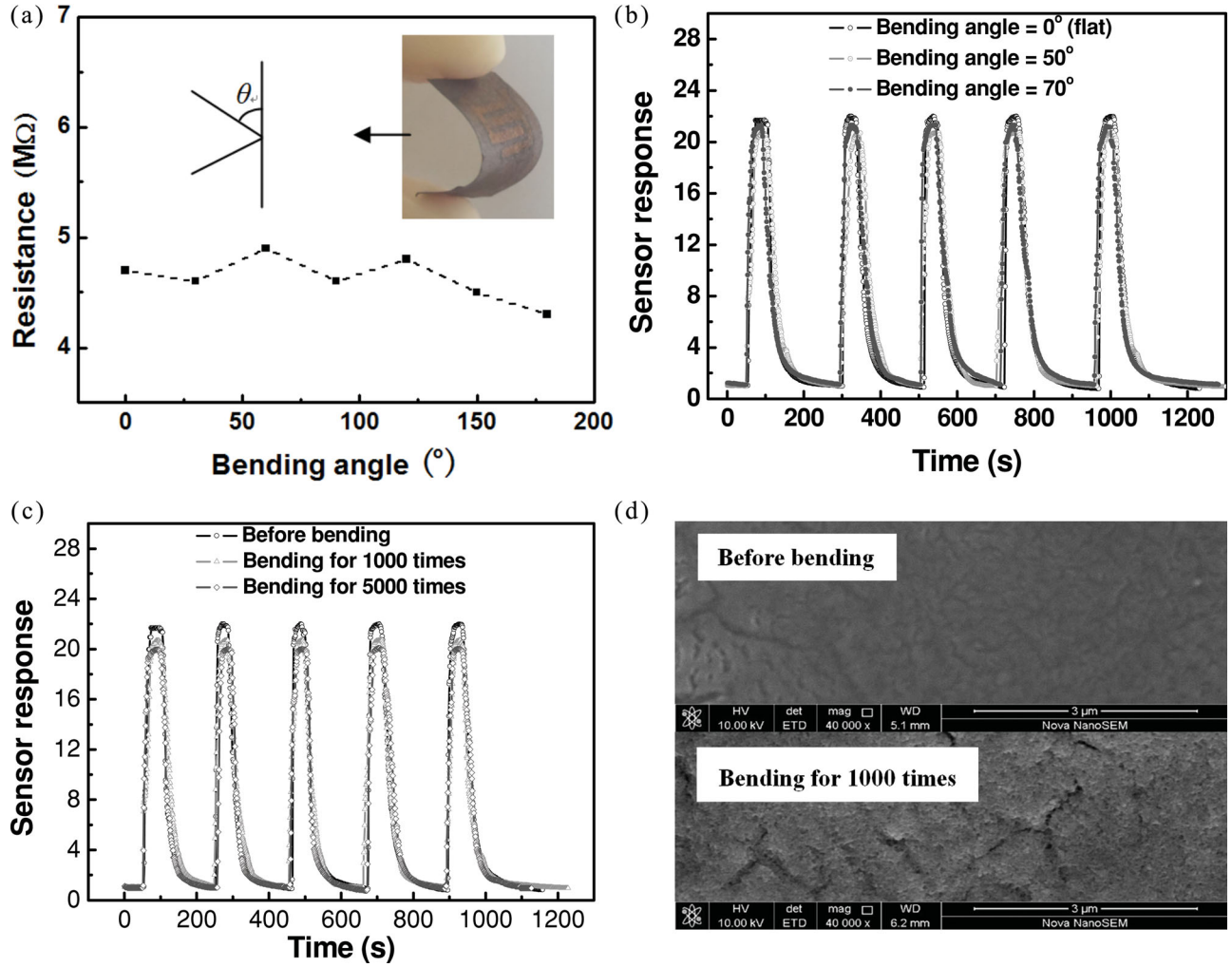

Figure 3. Flexibility of PbS CQD gas sensor on paper substrate. a) The resistance of the sensor in air under different bending angles. Inset: Image of the bent sensor. b) Response curves of the sensor to 50 ppm of NO_2 when tested under different bending angles. c) Response curves of the sensor tested before and after bending 1000 and 5000 times (bending angle = 50°). d) Top-view SEM images of the paper-based gas sensor before and after bending 1000 times.

Adv. Mater. **2014**,
DOI: 10.1002/adma.201304366

The device shows only a slight decrease in response (7.1% of the initial value) and identical temporal response when subjected to 5000 bending and unbending cycles. Scanning electron microscopy (SEM) analysis revealed a morphology change of the paper-based sensors caused by mechanical bending (Figure 3d). Before bending, a rough surface with small cracks was observed. After bending, the width and depth of cracks slightly increased, and the film remained continuous, beneficial for preserving its sensing performance to a large extent.

We now discuss the sensing mechanism of our PbS CQD gas sensors, first summarizing the relevant experimental observations.

First, a linear current–voltage (*I*–*V*) curve indicates ohmic contact between the PbS CQD film and Au electrodes (Figure S4, Supporting Information), and the resistance measurement as a function of electrode spacing confirmed that the measured resistance was dominated by the PbS CQD film rather than the contact resistance. We thus conclude that the sensor response upon gas exposure comes from the change of the resistance of the PbS CQD film itself.

Second, for comparison, we measured the gas response of bulk PbS film deposited by chemical bath deposition (**Figure 4**a). Unlike the $NaNO_2$-treated PbS CQDs, a very low but detectable response to 50 ppm of NO_2 at room temperature was observed, similar to reports in the literature.[26] We also measured the sensor response of PbS CQD film without the $NaNO_2$ methanol treatment and observed no response to NO_2 (Figure 4a). The 1.8 nm long oleate ligands form a tightly bound shell fully protecting the PbS CQDs surface. Xu et al. reported a similar observation where the gas response of their SnO_2 CQDs was substantially hindered by the abundant oleic acid and oleylamine capping ligand.[27] When most oleate ligands were removed by the $NaNO_2$ treatment, strong gas response was obtained. In addition, both our PbS CQDs and bulk PbS film[18] showed no response to NO_2 at temperatures higher than 70 °C.[26] We infer that the chemical nature of the interaction between PbS and NO_2 is not altered by the size reduction. We thus conclude that the higher response of $NaNO_2$-treated PbS CQDs compared to the bulk film is due to the enhanced accessibility of CQD surfaces to gas molecules.

Third, we found that sensor response was much higher when a higher Pb to S ratio was used in the precursor solutions (Pb:S = 4:1) during the synthesis (Figure 4b). Higher Pb to S ratio is expected to produce PbS CQDs with more Pb cations residing on the surface,[16] by which the adsorption of NO_2 molecules and interaction could be enhanced, which would be beneficial to sensing performance.

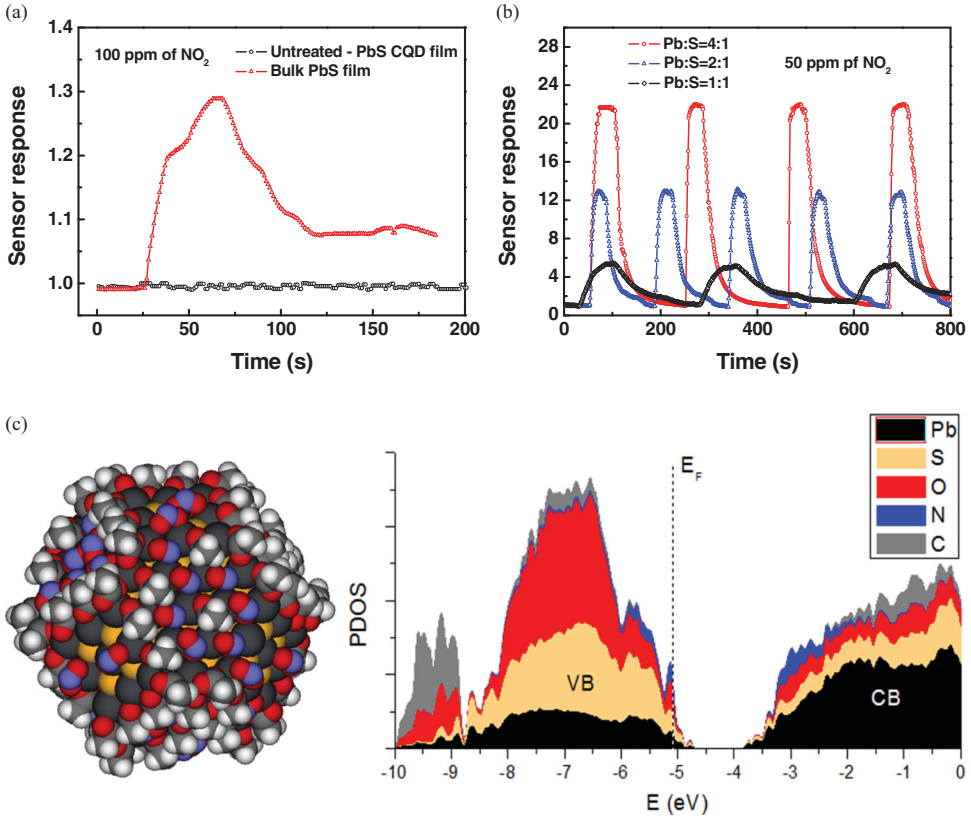

Figure 4. Sensing mechanism study. a) Response curves of the bulk PbS film and the untreated PbS CQD film to 50 ppm of NO_2. b) Sensor response of the fabricated device using PbS CQDs with different molar ratios of Pb and S. All devices were treated with 10 mg mL^{-1} $NaNO_2$ methanol solution and tested with 50 ppm of NO_2 gas at room temperature. c) Left: Schematic illustration of a PbS CQD with NO_2 and oleate passivation. Right: projected DOS for NO_2 binding to a PbS CQD surface (VB: valence band; CB: conduction band).

We employed density functional theory (DFT) simulations to investigate further the mechanism of NO_2 gas sensing. DFT simulations were performed using SIESTA code[28] (see computational methods in the Experimental Section for details). A Pb-rich PbS CQD of 2.4 nm size (ca. 400 atoms in the core) with oleate and NO_2 ligands was used for the simulation. As shown in Figure 4c, NO_2 behaves as a ligand, binding to surface Pb sites through its oxygen atoms. Calculations show that NO_2 introduces additional energy levels deep in the valence band, inducing p-type doping, similarly to adsorption of carboxy groups and of oxygen.[29] The projected density of states (DOS) is also presented in Figure 4c. The valence band edge remains core-like, indicating that NO_2 binding does not introduce trap states. The computed binding energy was calculated to be approximately 0.8 eV, much stronger than the estimated binding energy for O_2 on PbS CQDs (0.5 eV), confirming that incoming NO_2 molecules could easily replace O_2 molecules originally bonded to the PbS CQD surface. As in the case of halide ligands binding to PbS CQD surfaces in films based on 3-mercaptopropionic acid (MPA) ligand treatments,[30] NO_2 is sterically small and is readily adsorbed onto the surface in large amounts, maximizing the potential for transient increases of doping density. This estimated binding energy (0.8 eV), however, is about 4 times weaker than the binding energy of oleate ligands — consistent with the reversibility of the physisorption process in the sensor in contrast to the strong covalent binding of oleate ligands.

Taking together the above experimental observations and the results of DFT simulations, we are able to propose a more detailed model for the operation of the CQD gas sensors. PbS CQD film treated by $NaNO_2$ methanol solution produces a p-type film in ambient air, ohmically contacted via the Au electrode. Because of oleate ligand removal after $NaNO_2$ treatment, the PbS surface is largely exposed to the incoming gas molecules. As a result of its strong binding energy, NO_2 kicks out the originally physisorbed O_2 molecules and binds to Pb^{2+} through O, introducing more charge-transfer-driven p-type doping. Hole concentration in the p-type PbS CQD film increases after NO_2 exposure, resulting in the resistance decrease shown as the gas response. The large surface area of 4 nm CQDs facilitates sensitive response, and the thin and porous CQD film enables quick diffusion and hence rapid response. The short recovery time and completely reversible response is explainable by the modest binding energy of NO_2 molecules on the PbS CQD surface, which could be desorbed easily after pumping, yielding signal recovery.

We investigated the possibility of a direct correlation between the employment of NO_2^- in the treatment of the CQD films and their specific sensitivity to NO_2 gas. We used the same methanol-based solution treatment but instead employed a number of other inorganic salts. Experiments showed that for NO_2 gas sensing at room temperature, $Pb(NO_3)_2$ treatment yielded negligible response, NH_4Cl resulted in devices with stronger yet more sluggish response, and NaOH treatment produced similar device response in terms of sensitivity and speed as $NaNO_2$ treatment. The comprehensive investigation of the sensing mechanism of PbS CQD gas sensors treated by different salts is beyond the scope of this communication, but the strong dependence of sensing characteristics on salt treatment provides a versatile strategy to further improve PbS CQD device performance.

In conclusion, we have demonstrated a high performance, paper-based flexible NO_2 gas sensor using PbS CQDs. Thanks to its extremely large surface area and solution processing, the PbS CQD–based gas sensor showed excellent NO_2 sensing performance at room temperature, including rapid response and high sensitivity, good reversibility, and outstanding mechanical bending ability and robustness. Experimental and theoretical study revealed that NO_2 bonds to the PbS CQD surface, introducing p-type doping and resistance reduction. The small binding energy facilitates quick desorption of NO_2 from the PbS CQD surface, giving rise to the quick signal recovery. Employment of CQDs for high performance flexible gas sensors opens lots of opportunities in portable and even wearable gas sensing applications.

Experimental Section

PbS CQD synthesis: PbS CQDs were synthesized through reaction of Pb-oleate and bis(trimethylsilyl) sulfide (TMS) using a standard Schlenk line. Octadecene (ODE) was degassed by pumping at 80 °C for 8 h prior to use. PbO (1.8 g, 8.0 mmol), oleic acid (19.2 mol, 6 mL), and 1-octadecene (20 mL) were mixed in a three-neck flask and heated to 90 °C under vacuum for 8 h. The flask temperature was increased to 120 °C and then 280 μL TMS in 10 mL ODE was rapidly injected. After injection, the temperature dropped to 95 °C and the heating mantle was turned off. The flask was then transferred to a cold water bath for cooling down to 36 °C. The product was rinsed with acetone and finally dispersed in octane at a concentration of 50 mg mL^{-1}.

Sensor device fabrication: Materials for the device fabrication included PbS CQDs in octane (50 mg mL^{-1}), $NaNO_2$ diluted with methanol (10 mg mL^{-1}), and anhydrous methanol. The layer-by-layer spin-coating deposition technique was carried out on a spin coater inside a fume hood according to the following steps: 1) Three drops of PbS CQDs solution were dropped onto the substrates (paper, PET, and Al_2O_3) pre-patterned with interdigital Au electrodes and then spun at 2500 rpm for 15 s. 2) 1 mL of diluted $NaNO_2$ in methanol was added dropwise to the substrates. After a 45 s wait, they were spun at 2500 rpm for 10 s. The $NaNO_2$ treatment was repeated twice. 3) The film was washed by methanol flush and then spun dry three times. 4) Steps 1–3 were repeated twice.

General characterization: UV–vis absorption spectra were obtained using a PerkinElmer Lambda 950 UV/vis/NIR spectrophotometer. SEM characterization was carried out using a FEI Sirion 200 scanning electron microscope. FTIR spectra were obtained using a Bruker Vertex 70 infrared spectrometer. *I–V* curves were recorded using a Keithley 6487 picoammeter. A VG Systems MultiLab 2000 XPS system was used with a monochromated Al Kα radiation source (1486.7 eV) for the XPS examination. The binding energy scale was calibrated using the C 1s peak at 284.6 eV.

Gas-sensing measurement: The gas-sensing response curves of the sensor samples were measured using gas sensing characterization instrumentation (QMCS-I, Huazhong University of Science and Technology, P. R. China) where the samples were connected in series with a signal resistor (R_o) and mounted over the test-board in a chamber of 0.7 L volume (see the Supporting Information for more details). The static method was employed and the gas concentration was determined by the volume ratio. The gas sensing tests throughout the work were performed under atmospheric pressure to characterize the response to target gas in the concentration range of 0.5–50 ppm in air. The relative humidity values of the target gas and base air at 25 °C were both (45±1)%.

Adv. Mater. 2014,
DOI: 10.1002/adma.201304366

Computational methods: DFT simulations were performed using SIESTA code with atomic orbital basis set of double-zeta plus polarization quality and norm-conserving Troullier–Martins pseudopotentials with nonlinear core corrections. The generalized gradient approximation with Perdew–Burke–Ernzerhof (PBE) functional and charge density grid cutoff of 300 Ry was used. A Pb-rich CQD of 2.4 nm size (ca. 400 atoms in the core) with oleate and NO_2 ligands (the numbers of these two ligands are approximately identical) was constructed and relaxed until forces of 40 meV A^{-1} were reached. Several starting geometries were tested, with the amount of carboxylic ligands adjusted to exactly compensate the excess of Pb to achieve undoped structure and NO_2 ligands adsorbed on top, as well as NO_2 replacing the original carboxy moieties. Ligand binding energies were computed with corrections for basis set superposition errors.

Supporting Information

Supporting Information is available from the Wiley Online Library or from the author.

Acknowledgements

This work was financially supported by the National Natural Science Foundation of China (61006012 and 61274055) and by the Self-determined and Innovative Research Funds of HUST. J.T. and H.L. acknowledge the "National 1000 Young Talents" project and the Program for New Century Excellent Talents in University (NCET-12–0216), respectively. The authors thank Prof. M. Q. Zhu, for experimental help at the beginning of this research, and the Analytical and Testing Center of HUST and the Center of Micro-Fabrication and Characterization (CMFC) of WNLO for facility access. They also acknowledge Innovative Technology and Beijing Technology Science Co. Ltd for glovebox and thermal evaporator technical assistance, respectively. Computations were performed on the BlueGene/Q supercomputer at the SciNet HPC Consortium provided through the Southern Ontario Smart Computing Innovation Platform (SOSCIP). The SOSCIP multi-university/industry consortium is funded by the Ontario Government and the Federal Economic Development Agency for Southern Ontario, Canada.

Received: August 30, 2013
Revised: November 20, 2013
Published online:

[1] a) D. Briand, A. Oprea, J. Courbat, N. Barsan, *Mater. Today* **2011**, *14*, 416; b) A. Oprea, J. Courbat, N. Barsan, D. Briand, N. F. de Rooij, U. Weimar, *Sens. Actuators B* **2009**, *140*, 227; c) O. Monereo, M. Boix, S. Claramunt, J. D. Prades, A. Cornet, A. Cirera, P. Merino, C. Merino, *Procedia Eng.* **2011**, *25*, 1425.
[2] a) N. Yamazoe, *Sens. Actuators B* **2005**, *108*, 2; b) A. Afzal, N. Cioffi, L. Sabbatini, L. Torsi, *Sens. Actuators B* **2012**, *171*, 25.
[3] B. Hu, W. Chen, J. Zhou, *Sens. Actuators B* **2013**, *176*, 522.
[4] a) S. Ammu, V. Dua, S. R. Agnihotra, S. P. Surwade, A. Phulgirkar, S. Patel, S. K. Manohar, *J. Am. Chem. Soc.* **2012**, *134*, 4553; b) K. Lee, B. K. Ju, *Phys. Status Solidi A* **2012**, *209*, 2082.
[5] a) V. Dua, S. P. Surwade, S. Ammu, S. R. Agnihotra, S. Jain, K. E. Roberts, S. Park, R. S. Ruoff, S. K. Manohar, *Angew. Chem. Int. Ed.* **2010**, *49*, 2154; b) Y. Guo, B. Wu, H. Liu, Y. Ma, Y. Yang, J. Zheng, G. Yu, Y. Liu, *Adv. Mater.* **2011**, *23*, 4626.
[6] a) H. Liu, J. Wan, Q. Fu, M. Li, W. Luo, Z. Zheng, H. Cao, Y. Hu, D. Zhou, *Sens. Actuators B* **2013**, *177*, 460; b) J. Liu, Z. P. Guo, K. X. Zhu, W. J. Wang, C. F. Zhang, X. L. Chen, *J. Mater. Chem.* **2011**, *21*, 11412.
[7] Y. Qin, X. Sun, X. Li, M. Hu, *Sens. Actuators B* **2012**, *162*, 244.
[8] D. J. Yang, I. Kamienchick, D. Y. Youn, A. Rothschild, I. D. Kim, *Adv. Funct. Mater.* **2010**, *20*, 4258.
[9] a) J. Tang, K. W. Kemp, S. Hoogland, K. S. Jeong, H. Liu, L. Levina, M. Furukawa, X. H. Wang, R. Debnath, D. K. Cha, K. W. Chou, A. Fischer, A. Amassian, J. B. Asbury, E. H. Sargent, *Nat. Mater.* **2011**, *10*, 765; b) J. Tang, H. Liu, D. Zhitomirsky, S. Hoogland, X. Wang, M. Furukawa, L. Levina, E. H. Sargent, *Nano Lett.* **2012**, *12*, 4889.
[10] G. Konstantatos, M. Badioli, L. Gaudreau, J. Osmond, M. Bernechea, F. P. Garcia de Arquer, F. Gatti, F. H. L. Koppens, *Nat. Nanotechnol.* **2012**, *7*, 363.
[11] L. Bakueva, S. Musikhin, M. A. Hines, T. W. F. Chang, M. Tzolov, G. D. Scholes, E. H. Sargent, *Appl. Phys. Lett.* **2003**, *82*, 2895.
[12] A. Forleo, L. Francioso, S. Capone, P. Siciliano, P. Lommens, Z. Hens, *Sens. Actuators B* **2010**, *146*, 111.
[13] J. M. Luther, M. Law, M. C. Beard, Q. Song, M. O. Reese, R. J. Ellingson, A. J. Nozik, *Nano Lett.* **2008**, *8*, 3488.
[14] D. V. Talapin, J.-S. Lee, M. V. Kovalenko, E. V. Shevchenko, *Chem. Rev.* **2009**, *110*, 389.
[15] A. D. Yoffe, *Adv. Phys.* **2001**, *50*, 1.
[16] J. Tang, L. Brzozowski, D. A. R. Barkhouse, X. Wang, R. Debnath, R. Wolowiec, E. Palmiano, L. Levina, A. G. Pattantyus-Abraham, D. Jamakosmanovic, E. H. Sargent, *ACS Nano* **2010**, *4*, 869.
[17] I. Moreels, K. Lambert, D. Smeets, D. De Muynck, T. Nollet, J. C. Martins, F. Vanhaecke, A. Vantomme, C. Delerue, G. Allan, Z. Hens, *ACS Nano* **2009**, *3*, 3023.
[18] A. Nag, M. V. Kovalenko, J. S. Lee, W. Y. Liu, B. Spokoyny, D. V. Talapin, *J. Am. Chem. Soc.* **2011**, *133*, 10612.
[19] F. Schedin, A. K. Geim, S. V. Morozov, E. W. Hill, P. Blake, M. I. Katsnelson, K. S. Novoselov, *Nat. Mater.* **2007**, *6*, 652.
[20] G. Chen, T. M. Paronyan, E. M. Pigos, A. R. Harutyunyan, *Sci. Rep.* **2012**, *2*, 343.
[21] S. L. Ji, H. B. Wang, T. Wang, D. H. Yan, *Adv. Mater.* **2013**, *25*, 1755.
[22] S.-W. Choi, A. Katoch, G.-J. Sun, S. S. Kim, *Sens. Actuators B* **2013**, *181*, 446.
[23] M. C. McAlpine, H. Ahmad, D. Wang, J. R. Heath, *Nat. Mater.* **2007**, *6*, 379.
[24] W. Yuan, A. Liu, L. Huang, C. Li, G. Shi, *Adv. Mater.* **2013**, *25*, 766.
[25] L. You, X. He, D. Wang, P. Sun, Y. F. Sun, X. S. Liang, Y. Du, G. Y. Lu, *Sens. Actuators B* **2012**, *173*, 426.
[26] T. Fu, *Sens. Actuators B* **2009**, *140*, 116.
[27] X. Xu, J. Zhuang, X. Wang, *J. Am. Chem. Soc.* **2008**, *130*, 12527.
[28] J. M. Soler, E. Artacho, J. D. Gale, A. Garcia, J. Junquera, P. Ordejon, D. Sanchez-Portal, *J. Phys.: Condens. Matter.* **2002**, *14*, 2745.
[29] O. Voznyy, D. Zhitomirsky, P. Stadler, Z. Ning, S. Hoogland, E. H. Sargent, *ACS Nano* **2012**, *6*, 8448.
[30] A. H. Ip, S. M. Thon, S. Hoogland, O. Voznyy, D. Zhitomirsky, R. Debnath, L. Levina, L. R. Rollny, G. H. Carey, A. Fischer, K. W. Kemp, I. J. Kramer, Z. Ning, A. J. Labelle, K. W. Chou, A. Amassian, E. H. Sargent, *Nat. Nanotechnol.* **2012**, *7*, 577.